Appl Phys B (2011) 103:669–679
DOI 10.1007/s00340-010-4252-y

Applied Physics B
Lasers and Optics

Control of spontaneous emission from an RF-driven five-level atom in an anisotropic double-band photonic-band-gap reservoir

C. Ding · J. Li · X. Yang

Received: 6 July 2010 / Revised version: 3 September 2010 / Published online: 16 October 2010

Abstract The control of spontaneous emission from an radio-frequency (RF)-driven five-level atom embedded in a three-dimensional photonic crystal is investigated by considering the anisotropic double-band photonic-band-gap (PBG) reservoir. It is shown that, due to the coexistence of the PBG and the quantum interference effect induced by the RF-driven field, some interesting features, such as the spectral-line narrowing, the spectral-line enhancement, the spectral-line suppression and the occurrence of a dark line in spontaneous emission, can be realized by adjusting system parameters under the experimentally available parameter conditions. The proposed scheme can be achieved by use of an RF-driven field into hyperfine levels in rubidium atom confined in a photonic crystal. These theoretical investigations may provide more degrees of freedom to vary the spontaneous emission.

1 Introduction

It has been now well documented that spontaneous emission from an excited atom depends not only on the properties of the atomic system but also on nature of the surrounding environment, and more specifically on the density of states of the radiation field [1, 2]. The usual way to modify the spontaneous emission of an atom is to place it in different circumstances, such as in free space [3–7], optical cavity [8–10], an optical waveguide [11–13], a photonic-band-gap (PBG) material [14–16], or an otherwise modified reservoir [17, 18]. For atoms in free space, atomic coherence and quantum interference are the basic mechanisms for controlling the atomic spontaneous emission. In the past few years, considerable work [19–26] has been done on the control and modification of the spontaneous emission. The quenching of spontaneous emission in an open V-type atom was studied in [27]. Phase-dependent effects in spontaneous emission spectra in a Λ-type atom were presented in Ref. [28]. Li et al. [29, 30] investigated the features of spontaneous emission spectra in a multi-level atomic system by means of an external coherent magnetic field driving a hyperfine transition. In addition, Wang et al. [31] experimentally demonstrated the effects of spontaneously generated coherence in a rubidium atomic beam.

Recently, PBG structures have been shown to have different density of states compared with the free-space vacuum field [32, 33]. The rapid variations of the photon density of states and the inhibition of electromagnetic wave propagation in photonic crystals provide another way to modify and control the spontaneous emission, which may facilitate the advancement of optics and optoelectronics, and has many important applications [34, 35]. Certain studies have been done for an excited atom embedded in photonic crystals, but most of them focus on three or four-level atom systems [36, 37]. The effect of atomic position on the spontaneous emission and optical spectrum of a three-level atom embedded in a photonic crystal was studied by considering the coherent two-band PBG reservoir in Ref. [38]. Angelakis et al. [39] investigated the spontaneous emission, absorption, and dispersion properties of a Λ-type atom where one transition interacts near resonantly with a double-band photonic crystal. Tan and Li [40] studied the influence of the driving field on the upper population evolution of a four-

C. Ding (✉) · J. Li · X. Yang
Wuhan National Laboratory for Optoelectronics and School of Physics, Huazhong University of Science and Technology, Wuhan 430074, People's Republic of China
e-mail: clding2006@126.com

J. Li
e-mail: huajia_li@163.com
Fax: +86-27-87557477

level atom in photonic crystals, which contains two upper levels and two lower levels. Paspalakis et al. [41] considered a four-level atom of "tripod" configuration with two transitions coupled to separate reservoirs, they just focused on the influence of the density of mode (DOM) of the non-Markovian reservoir on the number of dark lines in the spontaneous emission spectrum, but not the effect of the driving field detuning. Sun et al. [42, 43] discussed the influence of both the driving field and the PBG reservoir on the spontaneous emission of a tripod four-level atom embedded in photonic crystals, but the two transitions coupled to the same PBG reservoir. To the best of our knowledge, previous studies for the atom embedded in photonic crystals were limited to the case of only one transition coupled to a PBG reservoir [38, 39] or two transitions coupled to the same modified reservoir [42, 43], however, no theoretical work has been reported that two atomic transitions are respectively coupled to the upper and lower bands of a double-band PBG reservoir.

In this paper, we propose a different point of view on varying the spontaneous emission through changing the relative position of the embedded atom in double-band PBG reservoir and the external RF-driven field. Of particular interest is the application of an external RF-driven field, as the RF field is more readily available and easier to control in comparison with an additional laser field, and this is a situation considered in this paper. In addition, a double-band PBG structure is more appealing than a single-band structure in real applications, because it allows the synchronous manipulation of two different atomic transitions. Under different conditions, we discuss the influence of the relative positions of the atomic transition frequencies from the band edges as well as the intensity and detuning of the external RF-driven field on the atomic spontaneous emission spectra in the free-space and PBG reservoirs. The changes of the relative positions and the external RF-driven field will impact strongly on the atomic spontaneous emission properties. Some interesting phenomena were found such as RF-induced dark line, RF-induced spectral-line narrowing and RF-induced spectral-line enhancement, which can be attributed to the quantum interference effect and coherent control of the RF-driven field. The variation of the atomic position and RF-driven field would lead to the change of the spontaneous emission spectra. We also illustrate the feasibility of our proposed scheme by considering experimentally accessible atomic configurations. In practical realization of controlling and modifying spontaneous emission, the system of atoms embedded in a double-band anisotropic PBG material in this paper is, in fact, experimentally more versatile than another system of atoms only coupled to a free vacuum field. This is due to the fact that the width of the band gap can be tailor designed to the levels of an atom in the fabrication of the PBG material. These results of the proposed scheme may provide a new degree of freedom to vary

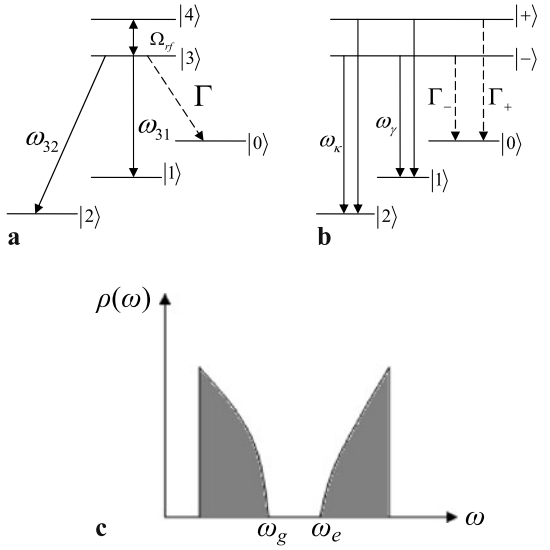

Fig. 1 (**a**) Schematic diagram of the five-level atomic system under consideration, which consists of three lower levels $|0\rangle$, $|1\rangle$, and $|2\rangle$, and two excited hyperfine levels $|3\rangle$ and $|4\rangle$. The transition frequencies ω_{31} and ω_{32} lie near the lower and upper band edges of the PBG, respectively, while the transition $|3\rangle \rightarrow |0\rangle$ is coupled by the vacuum-field mode in the free space, Γ denotes the decay rate. The hyperfine transition $|3\rangle \leftrightarrow |4\rangle$ is driven by an RF field with Larmor frequency $2\Omega_{\rm rf}$ which can produce strong dynamically induced coherence between them. (**b**) A corresponding dressed-state description of the RF-driven field. (**c**) The density of modes for the case of the double-band anisotropic PBG model

the spontaneous emission in PBG materials, especially for nonlinear optical phenomena.

The organization of this paper is as follows. In Sect. 2, the atomic model under consideration is presented. We apply the time-dependent Schrödinger equation to describe the interaction of our system with the modified reservoir and calculate the spontaneous emission spectra in the Markovian and non-Markovian reservoirs. In Sect. 3, we analyze and discuss the spontaneous emission properties of the system under different reservoirs. Also, we put forward the possible experimental realization of our scheme with cold ^{87}Rb atoms and three-dimensional photonic crystals. Finally, we conclude with a brief summary in Sect. 4.

2 Theoretical model and basic formula

We consider a five-level atom that consists of two upper levels $|3\rangle$ and $|4\rangle$, and three lower levels $|0\rangle$, $|1\rangle$, and $|2\rangle$ as depicted in Fig. 1(a). The DOMs for the double-band anisotropic PBG model with an upper band, a lower band, and a band gap as shown in Fig. 1(c). The atom is assumed to be initially in level $|3\rangle$ [39] via optical pumping. The transitions from the upper level $|3\rangle$ to the two lower levels $|1\rangle$ and $|2\rangle$ can be coupled by the double-band anisotropic PBG reservoir (this will be referred to as the non-Markovian

reservoir). The transition $|3\rangle \rightarrow |1\rangle$ is considered to be near resonant with the lower band edge of the PBG reservoir, and the transition $|3\rangle \rightarrow |2\rangle$ is taken to be near resonant with the upper band edge of the PBG reservoir, while the transition $|3\rangle \rightarrow |0\rangle$ is assumed to be far away from the PBG edges, and is coupled with the free-space reservoir (this will be referred to as the Markovian reservoir). An extra coherent field drives a hyperfine transition between two hyperfine levels $|3\rangle$ and $|4\rangle$, which can produce strong dynamically induced coherence between them. The two levels are located in the excited-state hyperfine structure, therefore the extra field is an RF-driven field with a carrier frequency $\omega_{\rm rf}$ and a Larmor frequency $2\Omega_{\rm rf}$ through an allowed magnetic dipole transition. The Hamiltonian which describes the dynamics of this system, in the interaction picture and the rotating wave approximation (RWA), is given by (taking $\hbar = 1$) [44–46]

$$\begin{aligned} H = {} & \Omega_{\rm rf} e^{i\Delta_{\rm rf} t} |3\rangle\langle 4| \\ & + \sum_{\lambda} g_{\lambda} e^{-i(\omega_{\lambda}-\omega_{30})t} |3\rangle\langle 0|\hat{a}_{\lambda} \\ & + \sum_{\gamma} g_{\gamma} e^{-i(\omega_{\gamma}-\omega_{31})t} |3\rangle\langle 1|\hat{a}_{\gamma} \\ & + \sum_{\kappa} g_{\kappa} e^{-i(\omega_{\kappa}-\omega_{32})t} |3\rangle\langle 2|\hat{a}_{\kappa} + \text{H.c.}, \end{aligned} \tag{1}$$

above the symbol H.c. stands for the Hermitian conjugate. $\Omega_{\rm rf}$ is one-half Larmor frequency of the external RF-driven field (assumed to be real for simplicity), i.e., $\Omega_{\rm rf} = \mu_{34} E_{\rm rf}/(2\hbar)$, with $\mu_{34} = \vec{\mu}_{34} \cdot \vec{e}_{\rm L}$ ($\vec{e}_{\rm L}$ is the unit polarization vector of the corresponding RF field) denoting the dipole matrix moment for the transition between levels $|3\rangle$ and $|4\rangle$. $\Delta_{\rm rf} = \omega_{\rm rf} - \omega_{43}$ represents the detuning of the external RF-driven field from resonant frequency of the $|3\rangle \leftrightarrow |4\rangle$ transition. Here g_{λ} characterizes the coupling constant of the atom with the free-space vacuum modes λ, and g_{γ} (g_{κ}) is the coupling constant between the lower (upper)-band-reservoir modes γ (κ) and the atomic transition from $|3\rangle$ to $|1\rangle$ ($|2\rangle$). These coupling constants are assumed to be real for simplicity. $\hat{a}_j$ and $\hat{a}_j^{\dagger}$ are the annihilation and creation operators for the jth reservoir modes with frequency ω_j ($j = \lambda, \gamma, \kappa$).

The description of the system is done via a probability amplitude approach. The state vector of the atomic system, at a specific time t, can be expanded in terms of the bare-state eigenvectors such that

$$\begin{aligned} |\Psi(t)\rangle = {} & b_3(t)|3\rangle|\{0\}\rangle + b_4(t)|4\rangle|\{0\}\rangle \\ & + \sum_{\lambda} b_{\lambda}(t)|0\rangle|1_{\lambda}\rangle + \sum_{\gamma} b_{\gamma}(t)|1\rangle|1_{\gamma}\rangle \\ & + \sum_{\kappa} b_{\kappa}(t)|2\rangle|1_{\kappa}\rangle, \end{aligned} \tag{2}$$

where $b_j(t)$ ($j = 3, 4, \lambda, \gamma, \kappa$) stands for the time-dependent probability amplitude of the atomic state, the initial value of which depends upon the initial quantum state of the atom being prepared. $|\{0\}\rangle$ denotes the vacuum of the radiation field, and $|1_{\lambda}\rangle$ indicates that there is one photon in the λth vacuum mode, $|1_{\gamma}\rangle$ ($|1_{\kappa}\rangle$) means that there is one photon in the $\gamma(\kappa)$th modified reservoir mode.

Substituting the interaction Hamiltonian and the atomic wave function of the system into the time-dependent Schrödinger equation $i\partial|\Psi(t)\rangle/\partial t = H_I|\Psi(t)\rangle$, the coupled equations of motion for the time evolution of the probability amplitudes can be readily obtained as

$$\begin{aligned} \frac{\partial b_3(t)}{\partial t} = {} & -i\Omega_{\rm rf} e^{i\Delta_{\rm rf} t} b_4(t) - i\sum_{\lambda} g_{\lambda} e^{-i(\omega_{\lambda}-\omega_{30})t} b_{\lambda}(t) \\ & - i\sum_{\gamma} g_{\gamma} e^{-i(\omega_{\gamma}-\omega_{31})t} b_{\gamma}(t) \\ & - i\sum_{\kappa} g_{\kappa} e^{-i(\omega_{\kappa}-\omega_{32})t} b_{\kappa}(t), \end{aligned} \tag{3a}$$

$$\frac{\partial b_4(t)}{\partial t} = -i\Omega_{\rm rf}^{*} e^{-i\Delta_{\rm rf} t} b_3(t), \tag{3b}$$

$$\frac{\partial b_{\lambda}(t)}{\partial t} = -i g_{\lambda}^{*} e^{i(\omega_{\lambda}-\omega_{30})t} b_3(t), \tag{3c}$$

$$\frac{\partial b_{\gamma}(t)}{\partial t} = -i g_{\gamma}^{*} e^{i(\omega_{\gamma}-\omega_{31})t} b_3(t), \tag{3d}$$

$$\frac{\partial b_{\kappa}(t)}{\partial t} = -i g_{\kappa}^{*} e^{i(\omega_{\kappa}-\omega_{32})t} b_3(t). \tag{3e}$$

We proceed by performing a formal time integration of (3c)–(3e) with respect to t' and substitute the results into (3a) to obtain the integrodifferential equation

$$\begin{aligned} \frac{\partial b_3(t)}{\partial t} = {} & -i\Omega_{\rm rf} e^{i\Delta_{\rm rf} t} b_4(t) \\ & - \int_0^t dt' b_3(t') \sum_{\lambda} g_{\lambda}^2 e^{-i(\omega_{\lambda}-\omega_{30})(t-t')} \\ & - \int_0^t dt' b_3(t') \sum_{\gamma} g_{\gamma}^2 e^{-i(\omega_{\gamma}-\omega_{31})(t-t')} \\ & - \int_0^t dt' b_3(t') \sum_{\kappa} g_{\kappa}^2 e^{-i(\omega_{\kappa}-\omega_{32})(t-t')}. \end{aligned} \tag{4}$$

Because the transition $|3\rangle \rightarrow |0\rangle$ is assumed to be far away from the PBG edges so that the density of states near ω_{30} is varied slowly, we can apply the usual Weisskopf–Wigner approximation [47, 48] and obtain

$$\sum_{\lambda} g_{\lambda}^2 e^{-i(\omega_{\lambda}-\omega_{30})(t-t')} = \frac{\Gamma}{2}\delta(t-t'), \tag{5}$$

where $\Gamma = 2\pi|g_{\lambda}|^2 D(\omega_{\lambda})$ is the spontaneous-decay rate from level $|3\rangle$ to level $|0\rangle$, and $D(\omega_{\lambda})$ is the vacuum-mode density at frequency ω_{λ} in the free space.

For the latter two summations in (4), they associated with the modified reservoir modes, the above result is not applicable as the DOMs of this reservoir is assumed to vary much more quickly than that of the free space. In order to solve this problem, we introduce the memory kernel [39]

$$K_{\gamma(\kappa)}(t-t') = \sum_{\gamma(\kappa)} g^2_{\gamma(\kappa)} e^{-i(\omega_{\gamma(\kappa)}-\omega_{31(32)})(t-t')}. \tag{6}$$

This equation depends very strongly on the photon density of states of the reservoir. In essence, the memory kernel is a measure of the photon reservoir's memory of its previous state on the time scale for the evolution of the atomic system, and it can be calculated using the appropriate DOM of the modified reservoir.

We consider the case of a double-band anisotropic effective-mass model of the PBG reservoir as shown in Fig. 1(c), which has an upper band, a lower band, and a band gap. The dispersion relations near the photonic-band edges are approximated by [1]

$$\begin{aligned} \omega_k &= \omega_g - A_g\left|(\vec{k}-\vec{k}_0)\right|^2, \quad \left|\vec{k}\right| < \left|\vec{k}_0\right|, \\ \omega_k &= \omega_e + A_e\left|(\vec{k}-\vec{k}_0)\right|^2, \quad \left|\vec{k}\right| > \left|\vec{k}_0\right|, \end{aligned} \tag{7}$$

where $A_j \approx \omega_j/|\vec{k}_0|^2$ $(j = g, e)$, ω_g and ω_e are the lower and upper frequencies at the edges of the band gap, respectively. Then, we have the following photonic DOMs at two band edges:

$$\rho_\gamma(\omega) \sim \sqrt{\omega_g - \omega}\,\Theta(\omega_g - \omega), \tag{8a}$$

$$\rho_\kappa(\omega) \sim \sqrt{\omega - \omega_e}\,\Theta(\omega - \omega_e), \tag{8b}$$

with the Heaviside step function Θ.

Under the effective-mass anisotropic dispersion relations (7), the kernel functions (6) can be expressed in the following forms [1]:

$$K_\gamma(t-t') = \alpha_{31}\frac{e^{i[\delta_g(t-t')-\pi/4]}}{\sqrt{4\pi(t-t')^3}}, \tag{9a}$$

$$K_\kappa(t-t') = \alpha_{32}\frac{e^{i[\delta_e(t-t')+\pi/4]}}{\sqrt{4\pi(t-t')^3}}, \tag{9b}$$

where $\alpha_{3j} \approx \frac{1}{4\pi\epsilon_0}\frac{\omega_{3j}^{5/2}\mu_{3j}^2}{3\hbar c^3}$ $(j = 1, 2)$ with the atomic dipole moment μ_{3j} for the transition $|3\rangle \to |j\rangle$, and $\delta_{g(e)} = \omega_{31(32)} - \omega_{g(e)}$ represents the detuning of the atomic transition frequency $\omega_{31}(\omega_{32})$ from the lower (upper) band-edge frequency $\omega_g(\omega_e)$.

Using (5) and (9) in (4), we can obtain

$$\begin{aligned} \frac{\partial b_3(t)}{\partial t} &= -i\Omega_{\rm rf}\tilde{b}_4(t) - \frac{\Gamma}{2}b_3(t) \\ &\quad - \int_0^t dt' b_3(t') K_\gamma(t-t') \\ &\quad - \int_0^t dt' b_3(t') K_\kappa(t-t'), \end{aligned} \tag{10}$$

here we have performed a change of variable $\tilde{b}_4(t) = e^{i\Delta_{\rm rf}t}b_4(t)$. Taking the Laplace transformations [48] $b_j(s) = \int_0^\infty e^{-st}b_j(t)\,dt$ for (3b) and (10), and s is the time Laplace transform variable, we have the results

$$s\tilde{b}_4(s) - \tilde{b}_4(0) = i\Delta_{\rm rf}\tilde{b}_4(s) - i\Omega^*_{\rm rf}b_3(s), \tag{11a}$$

$$\begin{aligned} sb_3(s) - b_3(0) &= -i\Omega_{\rm rf}\tilde{b}_4(s) - \frac{\Gamma}{2}b_3(s) \\ &\quad - b_3(s)K_\gamma(s) - b_3(s)K_\kappa(s), \end{aligned} \tag{11b}$$

where $K_{\gamma(\kappa)}(s)$ is the Laplace transform of $K_{\gamma(\kappa)}(t)$. From the above equations we can obtain

$$b_3(s) = \frac{b_3(0) - i\Omega_{\rm rf}b_4(0)/(s - i\Delta_{\rm rf})}{s + \Omega^2_{\rm rf}/(s - i\Delta_{\rm rf}) + \Gamma/2 + K_\gamma(s) + K_\kappa(s)}. \tag{12}$$

For the anisotropic band edges in the effective-mass approximation, the Laplace transforms of (9a) and (9b) are given by

$$\begin{aligned} K_\gamma(s) &= \alpha_{31}(-i\sqrt{is + \delta_g}), \\ K_\kappa(s) &= \alpha_{32}\sqrt{is + \delta_e}. \end{aligned} \tag{13}$$

Here, we first derive the long-time spontaneous emission spectra of the transition $|3\rangle \leftrightarrow |0\rangle$ within the Markovian reservoir, namely, $S(\delta_\lambda) \propto |b_\lambda(t \to \infty)|^2$ with the detuning frequency $\delta_\lambda = \omega_\lambda - \omega_{30}$. The long-time probability amplitude $b_\lambda(t \to \infty)$ could be also obtained from the final-value theorem $b_\lambda(t \to \infty) = \lim_{s\to 0}[sb_\lambda(s)]$ with $b_\lambda(s)$ being the Laplace transform of $b_\lambda(t)$ in Laplace variable s. Through performing the final-value theorem and Laplace transform, we have

$$\begin{aligned} S(\delta_\lambda) &= D(\omega_\lambda)|b_\lambda(t \to \infty)|^2 = \frac{\Gamma}{2\pi}|b_3(s = -i\delta_\lambda)|^2 \\ &= \frac{\Gamma}{2\pi}\left|\frac{b_3(0) + \Omega_{\rm rf}b_4(0)/(\delta_\lambda + \Delta_{\rm rf})}{-i\delta_\lambda + i\Omega^2_{\rm rf}/(\delta_\lambda + \Delta_{\rm rf}) + \Gamma/2 - i\alpha_{31}\sqrt{\delta_\lambda + \delta_g} + \alpha_{32}\sqrt{\delta_\lambda + \delta_e}}\right|^2. \end{aligned} \tag{14}$$

Then, we derive the long-time spontaneous emission spectra in the non-Markovian reservoir. The individual spectra associated with transitions $|3\rangle \to |1\rangle$ and $|3\rangle \to |2\rangle$ can be given by $S(\delta_\gamma) \propto |b_\gamma(t \to \infty)|^2$ and $S(\delta_\kappa) \propto |b_\kappa(t \to \infty)|^2$, respectively. We define the detuning frequencies as $\delta_\gamma = \omega_g - \omega_\gamma$ and $\delta_\kappa = \omega_\kappa - \omega_e$. Using the Laplace transform and final-value theorem, from (3d) and (3e) we can obtain

$$S(\delta_\gamma) = \rho_\gamma(\omega_\gamma)|b_\gamma(t \to \infty)|^2 \simeq |g_\gamma|^2\sqrt{\delta_\gamma}\left|\frac{b_3(0) - \Omega_{\rm rf}b_4(0)/(\delta_\gamma + \delta_g - \Delta_{\rm rf})}{\delta_\gamma + \delta_g - \Omega_{\rm rf}^2/(\delta_\gamma + \delta_g - \Delta_{\rm rf}) - i\Gamma/2 - i\alpha_{31}\sqrt{\delta_\gamma} + \alpha_{32}\sqrt{\delta_\gamma + \delta_g - \delta_e}}\right|^2, \tag{15a}$$

$$S(\delta_\kappa) = \rho_\kappa(\omega_\kappa)|b_\kappa(t \to \infty)|^2 \simeq |g_\kappa|^2\sqrt{\delta_\kappa}\left|\frac{b_3(0) + \Omega_{\rm rf}b_4(0)/(\delta_\kappa - \delta_e + \Delta_{\rm rf})}{\delta_\kappa - \delta_e - \Omega_{\rm rf}^2/(\delta_\kappa - \delta_e + \Delta_{\rm rf}) + i\Gamma/2 + \alpha_{31}\sqrt{\delta_\kappa - \delta_e + \delta_g} + i\alpha_{32}\sqrt{\delta_\kappa}}\right|^2. \tag{15b}$$

3 Result and discussion

In this section, we will discuss some properties about the atomic spontaneous emission spectra via a few numerical calculations based on (14) and (15) within the Markovian and non-Markovian reservoirs, respectively. All the parameters used in the following discussion are in units of γ, and γ is the decay rate for the transition from the upper level $|3\rangle$ to the lower level $|0\rangle$, i.e., $\Gamma = \gamma$, which should be in the order of MHz for rubidium atoms. Suppose that the atom is initially prepared in level $|3\rangle$ [39], i.e., $b_3(0) = 1$. In our scheme, the transitions from the level $|3\rangle$ to the two lower levels $|1\rangle$ and $|2\rangle$ are respectively coupled by the lower and upper bands of the PBG reservoir, and the transition $|3\rangle \leftrightarrow |4\rangle$ is coupled by the RF-driven field. These will lead to two possible types of quantum interferences. The first type is ascribed to the PBG modes, and the second one arises from the RF-driven field. As far as we know, there are no reports on the effects of the two types of quantum interferences on the spontaneous emission spectra for the case of transition from the upper level $|3\rangle$ to the lower level $|0\rangle$ coupled to the free vacuum modes and from level $|3\rangle$ to the lower level $|1\rangle$ ($|2\rangle$) coupled to the modified reservoir modes.

3.1 The spontaneous emission spectra in the Markovian reservoir

We begin with a study of the spontaneous emission spectra of the transition $|3\rangle \to |0\rangle$ within the Markovian reservoir. In the following, we will discuss the influence of the band-edge positions, as well as the detuning and intensity of the RF-driven field on the spontaneous emission spectra.

First of all, we analyze the influence of both the lower and upper band-edge positions on the spontaneous emission spectra, considering the detuning of the external RF-driven field as fixed and small, i.e., $\Delta_{\rm rf} = 1$. From Fig. 2, we can see that the spectral profile is fairly sensitive to the detunings of the atomic transition frequencies from the band edges. It is obvious that there exists two peaks and a dark line (zeros in the spectra at certain values of the emitted photon frequency). The dark line is located at $\delta_\lambda = -\Delta_{\rm rf}$ in Fig. 2, which originates from the RF-induced quantum interference. When one frequency ω_{31} for transition $|3\rangle \to |1\rangle$ is outside the band gap ($\delta_g = -2$) and the other ω_{32} for transition $|3\rangle \to |2\rangle$ is inside the gap ($\delta_e = -3$), the spectra exhibit a wider transparency window between two peaks, where the left peak is low and wide but the right one is high and narrow as shown in Fig. 2(a). However, for the case that the transition frequency ω_{31} moves deeply into the band gap ($\delta_g = 2$) and the transition frequency ω_{32} moves from the band gap to the upper band ($\delta_e = 2$), the sharp peak on the right-hand side is significantly suppressed while the small peak on the left-hand side is obviously enhanced compared with the situation inside the gap, as can be seen from Fig. 2(b). It is more interesting that when both transition frequencies of the atom are inside the band gap ($\delta_g = 2, \delta_e = -1.5$), the two peaks are enhanced and become narrower (see Fig. 2(c)). Whereas, when both transition frequencies are outside the gap ($\delta_g = -1.5, \delta_e = 2$), the two peaks are strongly suppressed and become wider (see Fig. 2(d)). These phenomena can be attributed to the nature of the three-dimensional

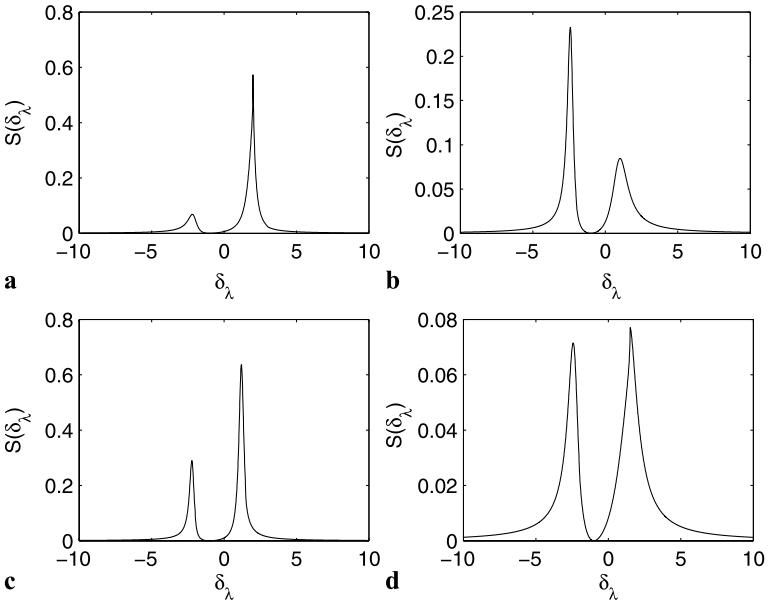

Fig. 2 The spontaneous emission spectra $S(\delta_\lambda)$ (in arbitrary units) for $\Gamma = 1$, $\alpha_{31} = \alpha_{32} = 0.5$, $\Omega_{\rm rf} = 2$, $\Delta_{\rm rf} = 1$, $b_3(0) = 1$, and $b_4(0) = 0$. (**a**) $\delta_g = -2$ and $\delta_e = -3$; (**b**) $\delta_g = 2$ and $\delta_e = 2$; (**c**) $\delta_g = 2$ and $\delta_e = -1.5$; and (**d**) $\delta_g = -1.5$ and $\delta_e = 2$

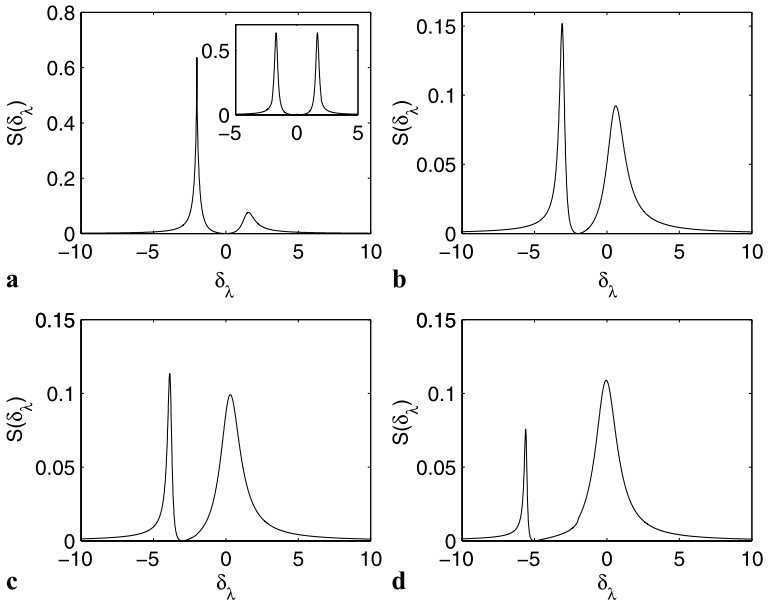

Fig. 3 The spontaneous emission spectra $S(\delta_\lambda)$ (in arbitrary units) for $\Gamma = 1$, $\alpha_{31} = \alpha_{32} = 0.5$, $\Omega_{\rm rf} = 2$, $b_3(0) = 1$, $b_4(0) = 0$, $\delta_g = 2$, and $\delta_e = 2$. The *inset* curve in (**a**) represents $\delta_g = 2$ and $\delta_e = -2$. (**a**) $\Delta_{\rm rf} = 0$; (**b**) $\Delta_{\rm rf} = 2$; (**c**) $\Delta_{\rm rf} = 3$; and (**d**) $\Delta_{\rm rf} = 5$

PBG material and the presence of the RF-driven field. In the following, we present a quantitative explanation for the preceding interesting phenomena of spontaneous emission in Fig. 2. In the language of dressed states, due to the presence of RF-driven field, the levels $|3\rangle$ and $|4\rangle$ can be replaced by two dressed levels $|+\rangle$ and $|-\rangle$, and then we can get a dressed-state system as shown in Fig. 1(b). Therefore, the spectra display double peaks for each transition from the dressed levels to the lower level $|0\rangle$, in which the destruction quantum interference between $|+\rangle \to |0\rangle$ and $|-\rangle \to |0\rangle$ leads to the appearance of the dark line.

Next, we will discuss how the frequency detuning of the RF-driven field modifies the spontaneous emission spectra for the atom embedded in the anisotropic PBG reservoir. Under the condition that the transition frequency ω_{31} lies in the band gap and the transition frequency ω_{32} within the upper band, in Fig. 3 we plot the spectra $S(\delta_\lambda)$ versus the detuning δ_λ by modulating the frequency of the RF-driven field. It is clearly shown that, when the RF-driven field is tuned to the resonant interaction with the atomic transition $|3\rangle \leftrightarrow |4\rangle$, an enhanced sharp peak and a small peak can be observed on both sides of zero detuning of δ_λ (see Fig. 3(a)). As in the case of non-resonance, the left peak is rapidly suppressed and the right peak is slightly enhanced compared with the situation at resonance (see Figs. 3(b)–3(d)). From these figures, we also find that the left-hand peak can be gradually decreased and becomes narrower, while the right-hand peak is slightly enhanced and becomes wider with the increase

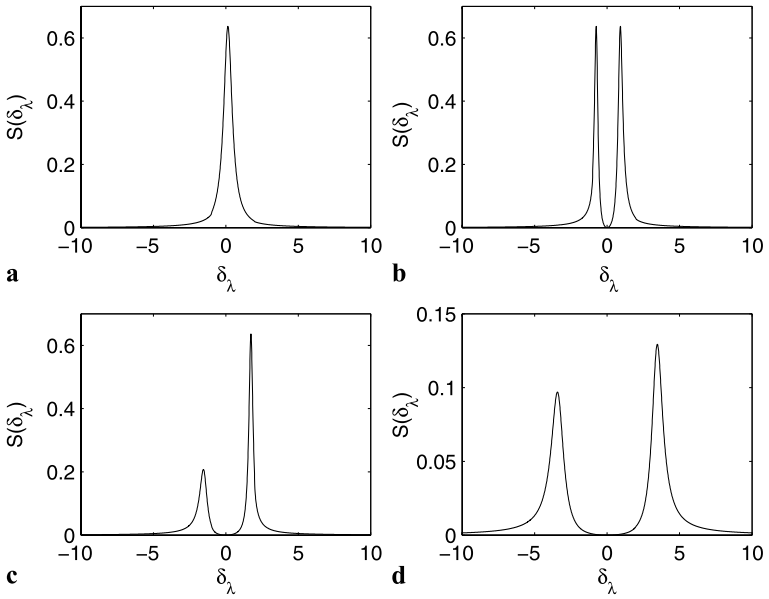

Fig. 4 The spontaneous emission spectra $S(\delta_\lambda)$ (in arbitrary units) for $\Gamma = 1$, $\alpha_{31} = \alpha_{32} = 0.5$, $\Delta_{\rm rf} = 0$, $b_3(0) = 1$, $b_4(0) = 0$, $\delta_g = 1$, and $\delta_e = -2$. (**a**) $\Omega_{\rm rf} = 0$; (**b**) $\Omega_{\rm rf} = 1$; (**c**) $\Omega_{\rm rf} = 2$; and (**d**) $\Omega_{\rm rf} = 4$

of the frequency detuning $\Delta_{\rm rf}$ of the RF-driven field. In addition, we observe that the separation between two peaks grows larger as the detuning increases. Finally, we would like to point out that, in other band-edge positions, similar results can be obtained (not shown here).

The reason for the appearance of the above phenomena in Fig. 3 can be explained by dressed-state theory. The dressed states $|+\rangle$ and $|-\rangle$ are the superposition of bare states $|3\rangle$ and $|4\rangle$. In the case of resonant excitations, the contribution of level $|3\rangle$ to the dressed state $|+\rangle$ is identical to that of $|-\rangle$, and in principle, the two peaks should be symmetrical with respect to the zero detuning of δ_λ. But as a matter of fact, the two peaks is not symmetric as shown in Fig. 3(a). This is mainly because one transition frequency lies inside the band gap and the other is outside the band gap, this asymmetrical internal structure leads to two asymmetrical peaks in the spectra. However, when both transition frequencies are inside or outside the band gap, moreover, the values of detuning between atomic transition and the corresponding band edge are equal (i.e., $|\delta_g| = |\delta_e|$), the spectra exhibit a symmetric double-peak structure (see the inset of Fig. 3(a)). In the meantime, as the detuning $\Delta_{\rm rf}$ increases, the contribution of level $|3\rangle$ to the dressed state $|-\rangle$ increases and the corresponding spontaneous emission relaxation rate from $|-\rangle$ to $|0\rangle$ increases, consequently, the right-hand peak in the spectra becomes wider. On the contrary, the contribution of level $|3\rangle$ to the dressed state $|+\rangle$ decreases, therefore the left-hand peak becomes narrower and lower.

In order to further explore the effect of the RF-driven field on the spontaneous emission spectra, we also plot $S(\delta_\lambda)$ versus the detuning δ_λ by adjusting intensities of the RF-driven field under the condition that both transition frequencies are inside the band gap ($\delta_g > 0, \delta_e < 0$) as shown in Fig. 4. As can be seen, the change of the RF-driven field intensity affects both the width and height of spectral lines, as well as the distance between two peaks. For the case that no RF-driven field exists ($\Omega_{\rm rf} = 0$), we can observe a Lorentzian shape in the spectra (see Fig. 4(a)). In contrast, for the case that the RF-driven field is applied, there exists two peaks and a dark line in the spectra as shown in Figs. 4(b)–4(d). Specifically, when the intensity of the RF-driven field is small (e.g., $\Omega_{\rm rf} = 1$), the spontaneous emission spectra exhibit symmetrical double-peak structure with equal height (see Fig. 4(b)). When the RF-driven field intensity continues to increase (e.g., $\Omega_{\rm rf} = 2$ in Fig. 4(c)), the left peak becomes wider and lower, while the right peak remains almost unchanged. It is worth mentioning that, only when the RF-driven field intensity is adjusted to strong enough (e.g., $\Omega_{\rm rf} = 4$ in Fig. 4(d)), the right-hand peak becomes wider and lower. In the meantime, the distance between two peaks grows larger as the intensity increases. This phenomenon is different from the spontaneous emission of multi-level atom embedded in isotropic photonic crystals [38, 39, 42, 43]. The reason for this should be attributed to the coexistence of the three-dimensional PBG material and the quantum interference effect induced by the RF-driven field during the spontaneous emission process.

3.2 The spontaneous emission spectra in the non-Markovian reservoir

We now turn to what happens to the spontaneous emission spectra associated with the transitions $|3\rangle \to |1\rangle$ and $|3\rangle \to |2\rangle$ within the non-Markovian reservoir. For the case that both of the transitions coupled to the same modified reservoir from a laser-driven four-level atom in photonic

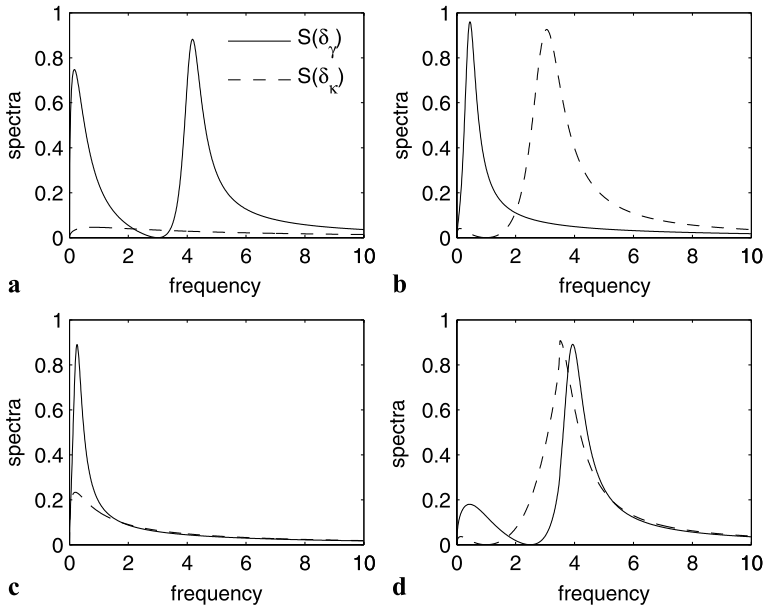

Fig. 5 The spontaneous emission spectra of separate transitions within non-Markovian reservoir. The *solid line* (*dashed line*) represents the spectral line associated with the transition $|3\rangle \to |1\rangle$ ($|3\rangle \to |2\rangle$). The parameters are $\Gamma = 1$, $\alpha_{31} = \alpha_{32} = 0.5$, $g_\gamma = g_\kappa = 1$, $\Omega_{\rm rf} = 2$, $\Delta_{\rm rf} = 1$, $b_3(0) = 1$, and $b_4(0) = 0$. (**a**) $\delta_g = -2$ and $\delta_e = -3.5$; (**b**) $\delta_g = 2$ and $\delta_e = 2$; (**c**) $\delta_g = 2$ and $\delta_e = -1.5$; and (**d**) $\delta_g = -1.5$ and $\delta_e = 2$

crystals has been discussed in Refs. [42, 43], and the case that one transition coupled to different band-reservoir modes from a three-level atom in a coherent PBG reservoir is also reported in Ref. [38]. However, the situation is quite different if one transition is coupled to the lower band and the other is coupled to the upper band in a double-band anisotropic PBG reservoir.

In the following, we shall consider how the spontaneous emission spectra are affected by the relative positions of the transition frequencies from the band edges, with the transitions $|3\rangle \to |1\rangle$ and $|3\rangle \to |2\rangle$ coupling to the lower and upper bands of the PBG reservoir, respectively. For fixed detuning of the RF-driven field, e.g., $\Delta_{\rm rf} = 1$, we plot the individual spectra in Fig. 5. As can be seen, when one transition frequency is within the lower band ($\delta_g = -2$) and the other lies inside the band gap ($\delta_e = -3.5$), the spontaneous emission spectra of transition $|3\rangle \to |1\rangle$ have two peaks and a dark line (zeros in the spectra at certain value) since the transition frequency ω_{31} is outside the band gap (solid line in Fig. 5(a)). For the $|3\rangle \to |2\rangle$ transition whose transition frequency ω_{32} lies in the band gap, the corresponding spectral line is suppressed strongly (dashed line in Fig. 5(a)). The physical interpretation of this phenomenon can be obtained from the dressed-state picture as shown in Fig. 1(b), due to the presence of the RF-driven field, the levels $|3\rangle$ and $|4\rangle$ can be replaced by two dressed levels $|+\rangle$ and $|-\rangle$, and then we can get a new triple-V five-level system. Therefore, the spectra show double peaks for each transition within non-Markovian reservoir, in which the RF-induced destructive quantum interference results in the appearance of the dark line. On the contrary, when the transition frequency ω_{31} lies inside the band gap, and the transition frequency ω_{32} is in the upper band, there only exists a single peak for the transition $|3\rangle \to |1\rangle$ (solid line in Fig. 5(b)). While the spontaneous emission spectra associated with transition $|3\rangle \to |2\rangle$ exhibit two peaks and a dark line (dashed line in Fig. 5(b)), similarly, the dark line is a resultant of the RF-induced destructive quantum interference. For the case that when both atomic transition frequencies are inside the band gap ($\delta_g > 0$, $\delta_e < 0$), the spontaneous emission from $|3\rangle$ to $|1\rangle$ is partially inhibited and the corresponding spectral line is a non-Lorentzian line shape, no dark line appears in the spectra because of the constructive quantum interference induced by the RF-driven field (solid line in Fig. 5(c)). The spontaneous emission spectra of $|3\rangle \to |2\rangle$ transition is the same as the dashed line in Fig. 5(a) and almost completely suppressed, where the long spectral tail should be an effect of $(\omega - \omega_e)^{1/2}$ dependence of the DOMs (dashed line in Fig. 5(c)). Figure 5(d) shows the individual spectra when both transition frequencies of the atom are outside the band gap ($\delta_g < 0$, $\delta_e > 0$), the individual spectral line presents a double-peak structure, in which one dark line appears. It can be seen from the five-level dressed-state system in Fig. 1(b), the spectra show two peaks for each transition within the non-Markovian reservoir, and the dark line originates from the RF-induced quantum interference.

In order to analyze the influence of the RF-driven field on the individual spectra, we give the corresponding curves by modulating frequencies of the RF-driven field under different positions of the band edges as shown in Figs. 6 and 7. The specific results are as follows. For the case that the transition frequency ω_{31} is outside the band gap and the transition frequency ω_{32} is inside the gap, two peaks and a dark line exist in the spontaneous emission spectra of transition $|3\rangle \to |1\rangle$, we find that the separation between two peaks grows larger as the detuning increases, and the right-hand

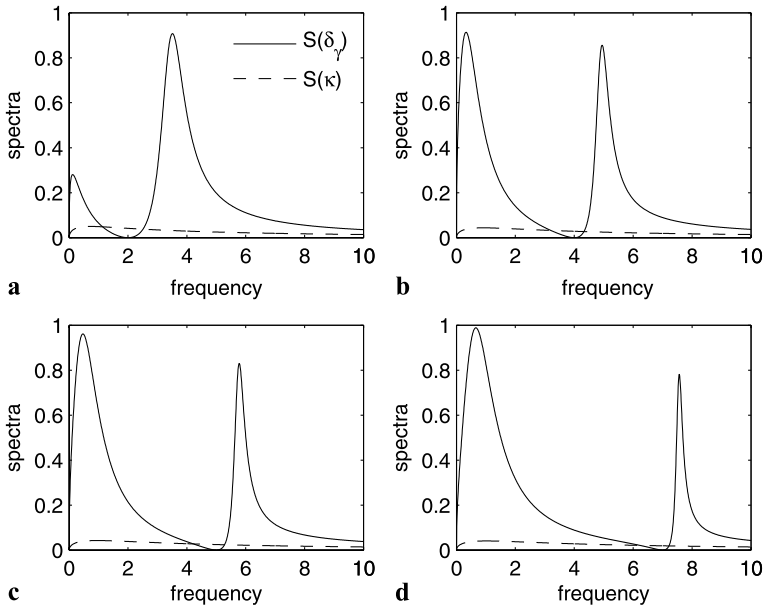

Fig. 6 The spontaneous emission spectra of separate transitions for various detuning. The parameters are $\Gamma = 1$, $\alpha_{31} = \alpha_{32} = 0.5$, $g_\gamma = g_\kappa = 1$, $\Omega_{\rm rf} = 2$, $b_3(0) = 1$, $b_4(0) = 0$, $\delta_g = -2$, and $\delta_e = -3.5$. (**a**) $\Delta_{\rm rf} = 0$; (**b**) $\Delta_{\rm rf} = 2$; (**c**) $\Delta_{\rm rf} = 3$; and (**d**) $\Delta_{\rm rf} = 5$

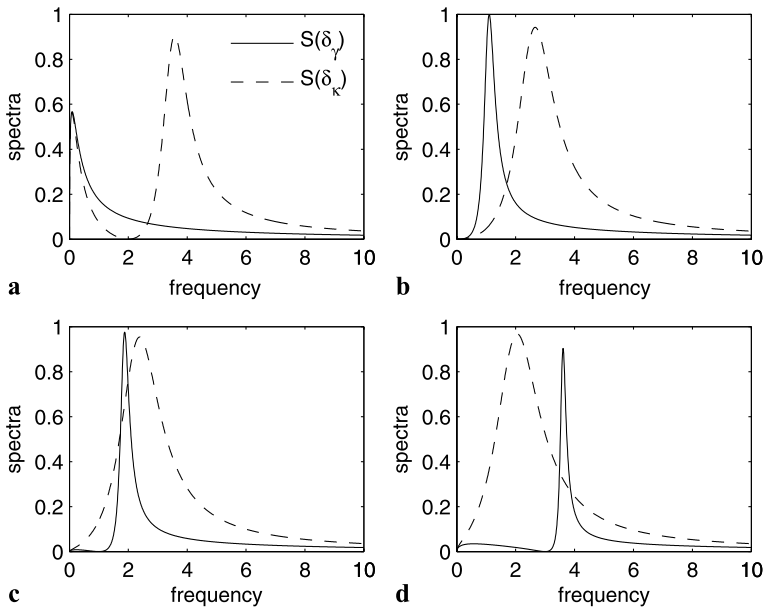

Fig. 7 The spontaneous emission spectra of separate transitions for various detuning. The parameters are $\Gamma = 1$, $\alpha_{31} = \alpha_{32} = 0.5$, $g_\gamma = g_\kappa = 1$, $\Omega_{\rm rf} = 2$, $b_3(0) = 1$, $b_4(0) = 0$, $\delta_g = 2$, and $\delta_e = 2$. (**a**) $\Delta_{\rm rf} = 0$; (**b**) $\Delta_{\rm rf} = 2$; (**c**) $\Delta_{\rm rf} = 3$; and (**d**) $\Delta_{\rm rf} = 5$

peak becomes narrower and lower, while the left-hand peak is slightly enhanced (solid line in Fig. 6). Since the transition frequency ω_{32} is inside the gap, the spontaneous emission of decay channel from $|3\rangle$ to $|2\rangle$ is suppressed strongly and the spectral line shows a strong non-Lorentzian line shape. That is, in this case, the detuning does not impact the decay property of this decay channel (dashed line in Fig. 6).

When the transition frequency ω_{31} lies inside the band gap and the transition frequency ω_{32} is outside the gap, the spectral line associated with transition $|3\rangle \to |1\rangle$ is of non-Lorentzian shape and the spectra of transition $|3\rangle \to |2\rangle$ show a double-peak structure in the case of resonance (see Fig. 7(a)). However, with the appearance of the detuning of the RF-driven field, the properties of individual spectra change greatly. For the inside-gap transition $|3\rangle \to |1\rangle$, the peak is rapidly enhanced and then becomes narrower and lower as the detuning increases, and keeps away from $\delta_\gamma = 0$ in the spectra, when the detuning is adjusted to large enough, a dark line emerges, thus the spectra display double-peak structure (solid line in Figs. 7(b)–7(d)). For the outside-gap transition $|3\rangle \to |2\rangle$, the left-hand peak in the spectra is completely suppressed in the non-resonant case, as the detuning increases, the right-hand peak is gradually close to $\delta_\gamma = 0$ (dashed line in Figs. 7(b)–7(d)). These phenomena are different from the case studied in Refs. [42, 43] where both of the transitions coupled to the same modified reservoir.

From what has been analyzed above, we can see that when the transition frequency ω_{31} is within the lower band, there will be a double-peak structure in the spectra for the transition $|3\rangle \rightarrow |1\rangle$ under any condition (solid line in Fig. 6). While for the case that the transition frequency ω_{31} lies inside the band gap, the corresponding spectra are of non-Lorentzian shape with a long spectral tail under resonance conditions (solid line in Fig. 7(a)), the spectra show a single-peak structure in the case of non-resonance (solid line in Figs. 7(b) and 7(c)), furthermore, when the RF-driven field detuning is adjusted to the appropriate value, there appears a double-peak structure in the spectra (solid line in Fig. 7(d)). The reason of these interesting phenomena can be explained by dressed-state theory. The dressed levels $|+\rangle$ and $|-\rangle$ are the superposition of bare levels $|3\rangle$ and $|4\rangle$. For the inside-gap transition $|3\rangle \rightarrow |1\rangle$, in the case of resonance, the contribution of level $|3\rangle$ to the dressed levels $|+\rangle$ is identical to that of $|-\rangle$ and the transition frequencies of $|+\rangle \rightarrow |1\rangle$ and $|-\rangle \rightarrow |1\rangle$ are equal but in the opposite direction within the band gap. However, as the detuning of the RF-driven field increases, the contribution of level $|3\rangle$ to the dressed level $|+\rangle$ decreases and the corresponding spontaneous emission from $|+\rangle$ to $|1\rangle$ decreases. On the contrary, the spontaneous emission from $|-\rangle$ to $|1\rangle$ increases, as a consequence, there will be one peak in the spectra (solid line in Figs. 7(a)–7(c)). However, when the detuning is tuned to large enough, the upper dressed level $|+\rangle$ is actually pushed out of the band gap and the lower dressed level $|-\rangle$ remains in the gap, therefore, there exhibits a double-peak structure in the spectra (solid line in Fig. 7(d)). While, for the outside-gap transition $|3\rangle \rightarrow |1\rangle$, two peaks corresponding to the decay channels $|+\rangle \rightarrow |1\rangle$ and $|-\rangle \rightarrow |1\rangle$, respectively. In addition, the dark line appears due to the destructive quantum interference between the two decay channels (solid line in Fig. 6). For the inside-gap transition $|3\rangle \rightarrow |2\rangle$, the spectral line is of non-Lorentzian shape, the detuning of the RF-driven field has no influence on the spectral property (dashed line in Fig. 6). However, when the transition frequency ω_{32} is within the upper band, the spectra display double-peak structure since the two transitions $|+\rangle \rightarrow |2\rangle$ and $|-\rangle \rightarrow |2\rangle$ are outside the band gap in the case of resonance (dashed line in Fig. 7(a)). But, as the detuning $\Delta_{\rm rf}$ increases, one dressed level is pushed into the band gap, thus the corresponding peak is completely suppressed, as a result, the spectra show a single-peak structure (dashed line in Figs. 7(b)–7(d)).

Before ending this section, let us briefly discuss the possible experimental realization of our proposed scheme by means of alkali-metal atoms, RF radiation source, and the double-band anisotropic photonic crystals. For example, we consider D_2 line of the cold ^{87}Rb atoms (nuclear spin $I = 3/2$) as a possible candidate. The designated states can be chosen as follows: $|0\rangle = |5S_{1/2}, F = 2, m_F = 2\rangle$, $|1\rangle = |5S_{1/2}, F = 2, m_F = 0\rangle$, $|2\rangle = |5S_{1/2}, F = 1, m_F = 1\rangle$, $|3\rangle = |5P_{3/2}, F = 2, m_F = 1\rangle$, and $|4\rangle = |5P_{3/2}, F = 3, m_F = 1\rangle$, respectively. In this case, an RF radiation field drives the magnetic dipole transition between $|3\rangle = |5P_{3/2}, F = 2, m_F = 1\rangle$ and $|4\rangle = |5P_{3/2}, F = 3, m_F = 1\rangle$ with the hyperfine splitting frequency $\omega_{34} \simeq 267.2$ MHz, while the transition from the excited level $|3\rangle = |5P_{3/2}, F = 2, m_F = 1\rangle$ to the lower levels $|1\rangle = |5S_{1/2}, F = 2, m_F = 0\rangle$ and $|2\rangle = |5S_{1/2}, F = 1, m_F = 1\rangle$ can be coupled by the lower and upper bands of the double-band anisotropic PBG reservoir, respectively. At the same time, the transition from the upper level $|3\rangle = |5P_{3/2}, F = 2, m_F = 1\rangle$ to the lower level $|0\rangle = |5S_{1/2}, F = 2, m_F = 2\rangle$ can be coupled by the vacuum-field mode in the free space.

4 Conclusions

In summary, we have studied and analyzed in details the properties of the spontaneous emission from an RF-driven five-level atom embedded in a double-band anisotropic PBG material. On the one hand, for the spontaneous emission spectra in the Markovian reservoir, there are two peaks and a dark line in the spontaneous emission spectra, and the separation between two peaks grows larger as the detuning or intensity of the RF-driven field increases. However, the spectra exhibit a single-peak structure in the absence of the RF field. On the other hand, for the spontaneous emission spectra in the non-Markovian reservoir, i.e., the transitions from the common upper level $|3\rangle$ to the two lower levels $|1\rangle$ and $|2\rangle$ interact with the lower and upper bands of the PBG reservoir, respectively, their corresponding individual spontaneous emission spectra also show interesting spectral properties: (i) For the transition $|3\rangle \rightarrow |1\rangle$, when the transition frequency ω_{31} occurs outside the band gap, or inside the gap but with a larger detuning of the RF-driven field, the spectral line is a double-peak structure. When the transition frequency ω_{31} is inside the band gap, the spectral line is a non-Lorentzian shape in the case of resonance, alternatively, the spectra display a single-peak structure for the small detuning of the RF-driven field. (ii) For the transition $|3\rangle \rightarrow |2\rangle$, when the transition frequency ω_{32} is inside the band gap, the spontaneous emission from level $|3\rangle$ to level $|2\rangle$ is suppressed strongly, therefore, the spectral line is of non-Lorentzian shape under any condition. For the case that the transition frequency ω_{32} is outside the band gap, when the frequency of the RF-driven field $\omega_{\rm rf}$ is in resonance with the corresponding transition, the spectral line shows a double-peak structure. In the case of non-resonance, there appears a single-peak structure in the spectra.

These results show that the spectral behaviors are very sensitive to the positions of the band edges and the variation of the RF-driven field, so we can control the spontaneous emission by adjusting these system parameters under

realistic experimental conditions. Finally, we would like to mention that the application of the RF-driven field in the MHz range offers us further flexibility to manipulate the light-matter interactions, including the control of spontaneous emission here, since the RF sources are more readily available and also provide a coherent, homogeneous and readily controllable radiation field. Therefore, according to our analysis, these interesting phenomena should be observable in realistic experiments by using cold Rb atoms, RF radiation source and three-dimensional PBG material.

Finally, we would like to point out that the use of photonic crystals to manipulate spontaneous emission contributes to the evolution of a variety of applications, including illumination, display, solar energy and even quantum-information systems. For example, in semiconductor lasers, spontaneous emission is the major sink for threshold current, which must be surmounted in order to initiate lasing. In some regions of the transistor current-voltage characteristic, spontaneous optical recombination of electrons and holes determines the heterojunction bipolar transistor current gain. In solar cells, spontaneous emission fundamentally determines the maximum available output voltage. In addition, it has many applications in quantum optics, optical communications, and in the fabrication of novel optoelectronic devices.

Acknowledgements We would like to thank Professor Ying Wu for helpful discussion and his encouragement. The research is in part supported by the National Natural Science Foundation of China (Grant Nos. 91021011, 10975054, 11004069 and 10874050), by the Doctoral Foundation of the Ministry of Education of China under Grant No. 200804870051 and by National Basic Research Program of China under Contract No. 2005CB724508. J.L. was also supported by the Innovation Foundation from Huazhong University of Science and Technology Under Grant No. 2010MS074.

References

1. M. Woldeyohannes, S. John, Phys. Rev. A **60**, 5046 (1999)
2. P. Lambropoulos, G.M. Nikolopoulos, T.R. Nielsen, S. Bat, Rep. Prog. Phys. **63**, 455 (2000)
3. S. John, T. Quang, Phys. Rev. Lett. **78**, 1888 (1997)
4. P. Zhou, S. Swain, Phys. Rev. A **55**, 772 (1997)
5. S.Y. Zhu, H. Chen, H. Huang, Phys. Rev. Lett. **79**, 205 (1997)
6. E. Paspalakis, C.H. Keitel, P.L. Knight, Phys. Rev. A **58**, 4868 (1998)
7. P. Zhou, S. Swain, Phys. Rev. Lett. **78**, 832 (1997)
8. E.M. Purcell, Phys. Rev. **69**, 681 (1946)
9. S. Haroche, J.M. Raimond, Adv. At. Mol. Phys. **20**, 347 (1985)
10. J.S. Peng, G.X. Li, P. Zhou, S. Swain, Phys. Rev. A **61**, 063807 (2000)
11. D. Kleppner, Phys. Rev. Lett. **47**, 233 (1981)
12. V. Frerichs, D. Meschede, A. Schenzle, Opt. Commun. **117**, 325 (1995)
13. G.X. Li, J. Evers, C.H. Keitel, Phys. Rev. B **80**, 045102 (2009)
14. T. Quang, M. Woldeyohannes, S. John, G.S. Agarwal, Phys. Rev. Lett. **79**, 5238 (1997)
15. Y.P. Yang, S.Y. Zhu, Phys. Rev. A **62**, 013805 (2000)
16. Y.P. Yang, M. Fleischhauer, S.Y. Zhu, Phys. Rev. A **68**, 043805 (2003)
17. C.W. Gardiner, Phys. Rev. Lett. **56**, 1917 (1986)
18. G.M. Palma, P.L. Knight, Phys. Rev. A **39**, 1962 (1989)
19. E. Paspalakis, N.J. Kylstra, P.L. Knight, Phys. Rev. A **61**, 045802 (2000)
20. F. Ghafoor, S. Qamar, M.S. Zubairy, Phys. Rev. A **65**, 043819 (2002)
21. Y. Wu, X. Yang, Phys. Rev. A **70**, 053818 (2004)
22. S.Y. Zhu, M.O. Scully, Phys. Rev. Lett. **76**, 388 (1996)
23. X.D. Sun, B. Zhang, X.Q. Jiang, Eur. Phys. J. D **55**, 699 (2009)
24. B.K. Dutta, P.K. Mahapatra, Phys. Scr. **79**, 065402 (2009)
25. B.K. Dutta, P.K. Mahapatra, Opt. Commun. **282**, 594 (2009)
26. J.H. Wu, A.J. Li, Y. Ding, Y.C. Zhao, J.Y. Gao, Phys. Rev. A **72**, 023802 (2005)
27. H. Lee, P. Polynkin, M.O. Scully, S.Y. Zhu, Phys. Rev. A **55**, 4454 (1997)
28. M.A.G. Martinez, P.R. Herczfeld, C. Samuels, L.M. Narducci, C.H. Keitel, Phys. Rev. A **55**, 4483 (1997)
29. J.H. Li, J.B. Liu, A.X. Chen, C.C. Qi, Phys. Rev. A **74**, 033816 (2006)
30. J.H. Li, Eur. Phys. J. D **42**, 467 (2007)
31. C.L. Wang, A.J. Li, X.Y. Zhou, Z.H. Kang, J. Yun, J.Y. Gao, Opt. Lett. **33**, 7 (2008)
32. E. Yablonovitch, Phys. Rev. Lett. **58**, 2059 (1987)
33. S. John, Phys. Rev. Lett. **58**, 2486 (1987)
34. E. Yablonovitch, J. Opt. Soc. Am. B **10**, 283 (1993)
35. J.D. Joannopoulos, R.D. Meade, J.N. Winn, *Photonic Crystals* (Princeton University Press, Princeton, 1995)
36. H. Huang, X.H. Lu, S.Y. Zhu, Phys. Rev. A **57**, 4945 (1998)
37. H.Z. Zhang, S.H. Tang, P. Dong, J. He, Phys. Rev. A **65**, 063802 (2002)
38. S.C. Cheng, J.N. Wu, T.J. Yang, W.F. Hsieh, Phys. Rev. A **79**, 013801 (2009)
39. D.G. Angelakis, E. Paspalakis, P.L. Knight, Phys. Rev. A **64**, 013801 (2001)
40. R. Tan, G.X. Li, J. Mod. Opt. **52**, 1729 (2005)
41. E. Paspalakis, D.G. Angelakis, P.L. Knight, Opt. Commun. **172**, 229 (1999)
42. X.D. Sun, X.Q. Jiang, Opt. Lett. **33**, 2 (2008)
43. X.Q. Jiang, B. Zhang, X.D. Sun, J. Phys. B: At. Mol. Opt. Phys. **41**, 065508 (2008)
44. Y. Wu, J. Saldana, Y. Zhu, Phys. Rev. A **67**, 013811 (2003)
45. Y. Wu, L. Wen, Y. Zhu, Opt. Lett. **28**, 631 (2003)
46. Y. Wu, X. Yang, Phys. Rev. A **71**, 053806 (2005)
47. V. Weisskopf, E.P. Wigner, Z. Phys. **54**, 63 (1930)
48. S.M. Barnett, P.M. Radmore, *Methods in Theoretical Quantum Optics* (Oxford University Press, Oxford, 1997)